Ocean Dynamics (2017) 67:23–36
DOI 10.1007/s10236-016-1013-4

Coastal sea level variability in the US West Coast Ocean Forecast System (WCOFS)

Alexander L. Kurapov[1] · **Svetlana Y. Erofeeva**[1] · **Edward Myers**[2]

Received: 1 June 2016 / Accepted: 28 October 2016 / Published online: 23 November 2016

Abstract Sea level variability along the US West Coast is analyzed using multi-year time series records from tide gauges and a high-resolution regional ocean model, the base of the West Coast Ocean Forecast System (WCOFS). One of the metrics utilized is the frequency of occurrences when model prediction is within 0.15 m from the observed sea level, *F*. A target level of $F = 90\%$ is set by an operational agency. A combination of the tidal sea level from a shallow water inverse model, inverted barometer (IB) term computed using surface air pressure from a mesoscale atmospheric model, and low-pass filtered sea level from WCOFS representing the effect of coastal ocean dynamics (DYN) provides the most straightforward approach to reaching levels $F>80\%$. The IB and DYN components each add between 5 and 15% to *F*. Given the importance of the DYN term bringing *F* closer to the operational requirement and its role as an indicator of the coastal ocean processes on scales from days to interannual, additional verification of the WCOFS subtidal sea level is provided in terms of the model-data correlation, standard deviation of the band-pass filtered (2–60 days) time series, the annual cycle amplitude, and alongshore sea level coherence in the range of 5–120-day periods. Model-data correlation in sea level increases from south to north along the US coast. The rms amplitude of model sea level variability in the 2–60-day band and its annual amplitude are weaker than observed north of 42 N, in the Pacific Northwest (PNW) coast region. The alongshore coherence amplitude and phase patterns are similar in the model and observations. Availability of the multi-year model solution allows computation and analysis of spatial maps of the coherence amplitude. For a reference location in the Southern California Bight, relatively short-period sea level motions (near 10 days) are incoherent with those north of the Santa Barbara Channel (in part, due to coastal trapped wave scattering and/or dissipation). At a range of periods around 60 days, the coastal sea level in Southern California is coherent with the sea surface height (SSH) variability over the *shelf break* in Oregon, Washington, and British Columbia, more than with the coastal SSH at the same latitudes.

Keywords Ocean modeling · Coastal sea level · Coastally trapped waves · US West Coast

Responsible Editor: Birgit Andrea Klein

✉ Alexander L. Kurapov
kurapov@coas.oregonstate.edu

[1] College of Earth, Ocean, and Atmospheric Sciences, Oregon State University, Corvallis, OR, USA

[2] Coast Survey Development Laboratory (CSDL), National Oceanic and Atmospheric Administration, 1315 East-West Highway, Silver Spring, MD 20910, USA

1 Introduction

To enable prediction and forecasts of oceanic conditions along the US West Coast, the Operational Ocean Forecast System (WCOFS) is being developed and tested at the Coast Survey Development Lab (CSDL), US National Oceanic and Atmospheric Administration (NOAA). It is based on the Regional Ocean Modeling System (www.myroms.org). To represent correctly local and remote forcing mechanisms of shelf flows along the US coast (32.5–49 N), the domain is stretched from 24 N (Southern Baja, Mexico) to 55 N (British Columbia, Canada) in the alongshore direction and 700–1000 km in the offshore direction (Fig. 1). The system will eventually include data assimilation and provide important information about currents, temperature, and salinity over the shelf,

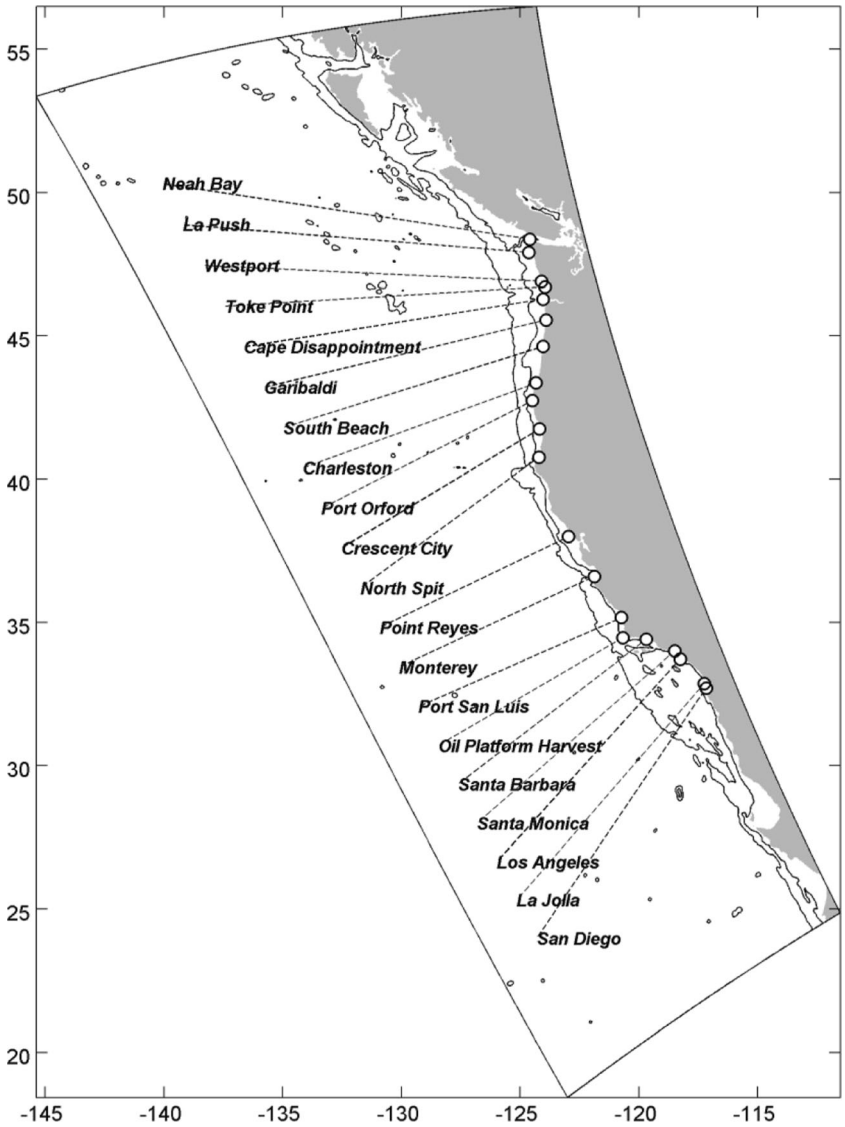

Fig. 1 Map: tide gauges locations, bathymetric contours at 200 and 2000 m.

continental slope, and adjacent interior ocean in support of navigation, fisheries, search and rescue, and environmental hazard response. As part of this effort, we also attempt to obtain an accurate, high-resolution, dynamically balanced, multiyear solution to facilitate skill assessment on seasonal and interannual temporal scales, reveal possible model biases, accumulate model error statistics for future data assimilation efforts, and perform valuable scientific analyses with focus on connectivity of processes along the US West Coast.

NOAA requires that the operational models predict accurately sea level variations along the coast to help navigation in estuaries and guide inundation and coastal wave forecasts. With focus on tide-dominated environments, a skill assessment protocol for the predicted water level has been put in place (Zhang et al. 2006), in which one of key metrics, F, is defined as the fraction (percentage) of times when the model-predicted sea level is within X meters from that observed by coastal tide gauges. The recommended threshold level, adopted in our analyses below, is X=0.15 m, and the acceptable level of F is near 90 % .This metric is called a "central frequency" by Zhang et al. (2006). We will discuss later sea level coherence, where the term *central frequency* can be naturally used to refer to the center of a frequency band. To avoid confusion, metrics F can be called here a *frequency of occurrence*.

While tide is a significant contributor to the total sea level along the West Coast, it is not strictly a tide-dominated environment. The tidal sea level range is on the order of ±1–2 m. The static effect of the time-variable barometric pressure on the ocean surface, or the inverse barometer (IB) effect (Wunsch and Stammer 1997), is on the order of 0.1 m and is relatively larger during extreme events, such as passing storms. For instance, extreme extratropical cyclones recorded along the US West Coast (Mass and Dotson 2010) may be associated with larger than 50 hPa drops in pressure, translating into a 0.5-m SSH rise. The dynamical adjustment (DYN) of the sea level to wind-driven shelf scale currents, eddies, and coastally trapped

waves (CTWs) can also add ±0.1 to 0.2 m to the coastal sea level variability at subinertial temporal scales (e.g., Springer et al. 2009; Kurapov et al. 2011). In particular, CTWs are forced by the winds and propagate from the south to north, resulting in coherent pattern of SSH variability at low frequencies along the US West Coast (e.g., Allen and Denbo 1984; Brink 1991; see discussion and additional references in section 5).

Some other processes not mentioned above can also influence coastal sea level measurements, for instance steric sea level variations associated with the sea water thermal expansion on seasonal to climatic temporal scales. Mellor and Ezer (1995) estimate that globally averaged seasonal change associated with this effect is small, on the order of 0.01 m. Evaluation of the steric effect in limited area regional models is difficult because of uncertainties in the open boundary horizontal volume, heat, and material fluxes.

The goal of this paper is to demonstrate that along the US West Coast the non-tidal components IB and DYN provide a measurable contribution to *F*, a metric that has previously been used by the operational oceanographers mostly for tide-dominating environments. In particular, we would like to demonstrate that WCOFS is a useful predictor of the DYN effect (section 3). Using a 6-year-long simulation and available tide gauge data, we also provide comparative analyses of the model subtidal sea level variability along the entire US West Coast in terms of additional metrics, including model-data correlations, standard deviations, the annual cycle amplitude (section 4), and alongshore coherence for a range of periods from 5 to 120 days (section 5). The model provides opportunity to compute two-dimensional SSH coherence maps, e.g., revealing details of the cross-shore structure of the alongshore traveling signal over realistic bathymetry; useful examples are discussed in section 5.

2 The model and data

The Regional Ocean Modeling System (ROMS, www.myroms.org) is a fully nonlinear, three-dimensional, hydrostatic, free-surface, Boussinesq ocean model featuring terrain-following coordinates in the vertical and advanced numerics (Shchepetkin and McWilliams 2003, 2005). The Mellor-Yamada (1982) option is chosen for vertical subgrid turbulence parameterization. The model domain is shown in Fig. 1. It extends from 24 N (Baja Peninsula) to 55 N (north of Queen Charlotte Bay, British Columbia) in the alongshore direction and 700–1000 km from the coast in the offshore direction. The model grid is regularly geographical in spherical coordinates rotated on the globe by placing the pole at 57.6°W, 37.4°N. The resolution is approximately 2 km in horizontal and 40 layers in the vertical direction, with at least 10 layers in the top 50 m. The horizontal Laplacian dissipation for momentum is 2 $m^2\ s^{-1}$ and the horizontal diffusion for the tracer fields is 0.1 $m^2\ s^{-1}$. A 100-km-wide sponge layer is implemented around the open boundaries, in which the horizontal dissipation is increased linearly to 200 $m^2\ s^{-1}$ toward the domain boundary, to dampen unwanted boundary effects.

The model is forced using a bulk flux formulation (Fairall et al. 1996). The required atmospheric fields (wind speed and direction, net shortwave radiation, downward longwave radiation, air temperature, relative humidity, and surface air pressure) are obtained by interpolation from the 12-km resolution NOAA Northern American Mesoscale Forecast System (NAM: grid 218, forecast archives with 3-h temporal resolution). The freshwater river discharges are included from the Columbia River (at the Oregon-Washington boundary, 46.2 N), the Fraser River (British Columbia), and 15 small rivers entering Puget Sound and Juan de Fuca Strait in Washington. Subtidal boundary conditions are obtained from the US Navy 1/12th degree resolution global ocean data assimilation system based on the Hybrid Coordinate Ocean Model (HYCOM, www.hycom.org); this global model did not include tidal forcing. A 5-day half-amplitude filter is applied to the HYCOM time series fields comprised of a series of snapshots once a day to reduce the effect of inertial motion aliasing and day-to-day noise possibly associated with instantaneous data assimilation corrections in the Navy model. Tides are added at the open boundaries using the tidal sea level and barotropic velocity amplitudes and phases for the eight dominant tidal constituents (including M_2, S_2, N_2, K_2, O_1, K_1, P_1, and Q_1). These were sampled from the 1/12th degree resolution tidal model solution for the Pacific basin (http://volkov.oce.orst.edu/tides/PO.html), which was constrained by assimilation of satellite altimetry in the Oregon State University Inverse Tidal Software (OTIS: Egbert and Erofeeva 2002; Erofeeva et al. 2003). The tidal boundary amplitudes and phases were corrected using nodal factors appropriate for our study interval.

The time and space-variable air pressure *P* at the sea surface was not included as the dynamic surface boundary condition, for consistency with the HYCOM boundary conditions. Its contribution to the changes in the total sea level is computed as the static IB response $(-(P - P_{MEAN})/(g\rho)$, where P_{MEAN} is the time-averaged sea level pressure, *g* gravity, and ρ the water density).

The model initial conditions are obtained by interpolation of the global HYCOM solution to the ROMS grid on 1 October 2008. After a 2-month spin-up period, a 1-year time series (1 December 2008 through 1 December 2009) was chosen for the metric *F* analyses (section 3); 6-min resolution time series of SSH have been recorded at selected locations for direct comparison with coastal tide gauge data. To further assess variability in the coastal SSH at relatively long, subtidal temporal scales (i.e., the DYN component), the model has been run without tides for a period of 1 October 2008–31 December 2014 and daily averaged model fields have been saved for analysis (sections 4 and 5).

Assessments of the WCOFS model were performed using model-data comparisons similar to those for a precursor model (Durski et al. 2015) and showed similarly good skill reproducing variability in the coastal currents, temperature, and other variables on temporal scales from days to seasonal and interannual. The present publication includes only evaluations for the coastal SSH. Verification of the WCOFS shelf currents, temperature, and salinity will be reported elsewhere.

The tide gauge observations, with 6-min temporal resolution, are obtained from the Center for Operational Oceanographic Products and Services (CO-OPS, http://tidesandcurrents.noaa.gov/). Stations utilized in this research are mapped in Fig. 1. Data gaps over the 6-year study period are infrequent, do not exceed 1 month, and never occur at neighboring stations simultaneously. These gaps have been filled by interpolation between the neighboring sites.

3 The subtidal sea level contribution to the frequency of occurrence metric (*F*)

WCOFS does predict the phase of the tidal sea level oscillations correctly, but the amplitudes near the coast are 10–20% lower than observed (not shown). This was in fact expected. The alongshore extent of the WCOFS domain (approximately 5000 km) is comparable to the wavelength of the semidiurnal M_2 and other dominant barotropic tidal constituents. To accurately predict tidal elevation amplitudes along the coast, application of both tidal boundary conditions and the interior volume forcing (tidal potential) would be necessary. However, the standard ROMS applies the tides only as boundary conditions, so WCOFS in this configuration will not be useful for the tidal sea level prediction along the coast. An accurate estimate of the tides is provided by the OTIS tidal model anyways, and this can be used for operational prediction of the total level if an accurate estimate of the DYN component can be obtained by WCOFS and IB by inverting the sea level pressure from the NAM atmospheric model.

The non-tidal contributions to the coastal sea level variation are measurable. To provide an example, for the South Beach (Oregon) location, the 13-month time series of the IB constituent is computed directly from the NAM *P* and the subtidal DYN constituent as the low-pass filtered WCOFS SSH using a 40-day half-amplitude filter (Fig. 2a). Episodic rising by 0.2 m due to the atmospheric pressure variations are apparent, e.g., during the passage of low pressure storm systems in December 2008–April 2009. SSH depressions of similar magnitude due to high pressure anomalies, lasting at least for a week, are also not uncommon in winter, e.g., showing twice in January 2009. A 0.3-m spike in IB due to a storm passing on 14 October 2009 is one of the most pronounced in this record. The ocean non-tidal dynamic effect represented by the WCOFS solution shows variations of similar amplitude (Fig. 2a, half-tone). In Oregon (OR), as well as in Northern California (CA) and Washington (WA), winds are predominantly northward, downwelling-favorable in winter and southward, upwelling-favorable in summer (e.g., Durski et al. 2015). So in winter, shelf currents are predominantly northward and SSH is rising along the coast. In spring and summer, the currents turn to the south and the sea level next to the coast lowers. During periods of wind relaxation or reversal, SSH relaxes as well.

Given the limited ability of the regional size ROMS application to predict accurately the tidal sea level, a practical solution toward accurate prediction of the total sea level requires combining terms from different sources:

$$\zeta(t) = \zeta_0 + \sum_k a_k \cos(\omega_k t - \varphi_k) + \zeta_{IB}(t) + \zeta_{DYN}(t) \qquad (1)$$

Here, ζ_0 is the reference level chosen to match the mean observed level. The second term in (1) is the sum of the tidal components with the amplitudes $a_k$and phases φ_k obtained by interpolation (or sometimes extrapolation) of the OTIS Pacific Basin solution at the tide gauge locations; these are corrected for our study period using nodal factors. ζ_{IB} is the IB correction computed using the sea level atmospheric pressure from NAM and ζ_{DYN} the ocean dynamic component, obtained as the low-pass filtered WCOFS SSH.

The IB and DYN effects are often of the same sign as, for instance, at the end of January 2009 when ζ_{IB} and ζ_{DYN} are both decreased, resulting in a larger than 0.3 m depression along the coast (see Fig. 2a). Figure 2b shows the time series of the observed total coastal sea level at the same tide gauge station during this event (half-tone line). By comparison, the estimate based only on the mean reference level and OTIS tides (dashed) is higher, while the total estimate based on (1) (solid black) is very close to the observations.

Similarly, during the storm of 14 October, the SSH rises both due to the IB effect and the cross-shore SSH slope adjustment to the intensified northward coastal current (see Fig. 2a). During this event, the tide-only estimate was lower than the observed total level (Fig. 2c), and $\zeta_{IB}(t) + \zeta_{DYN}(t)$ provides just enough correction to bring the prediction and observations in agreement.

To assess the impact of the IB and DYN terms on the predicted coastal sea level over the 1-year time interval, we next proceed with analysis of the frequency of occurrence metrics *F* (recall, defined as the percentage of times when the estimated sea level is within 0.15 m from observed). In particular, we would like to show that $\zeta_{IB}(t) + \zeta_{DYN}(t)$ helps reaching acceptable levels in *F*. At each tide gauge station along the US West Coast, this metrics was computed using the tide only estimate (the first two terms in (1); light gray bars in Fig. 3), tides plus the IB effect (the first three terms in (1); dark gray bars in Fig. 3), and all the four terms in (1) (black

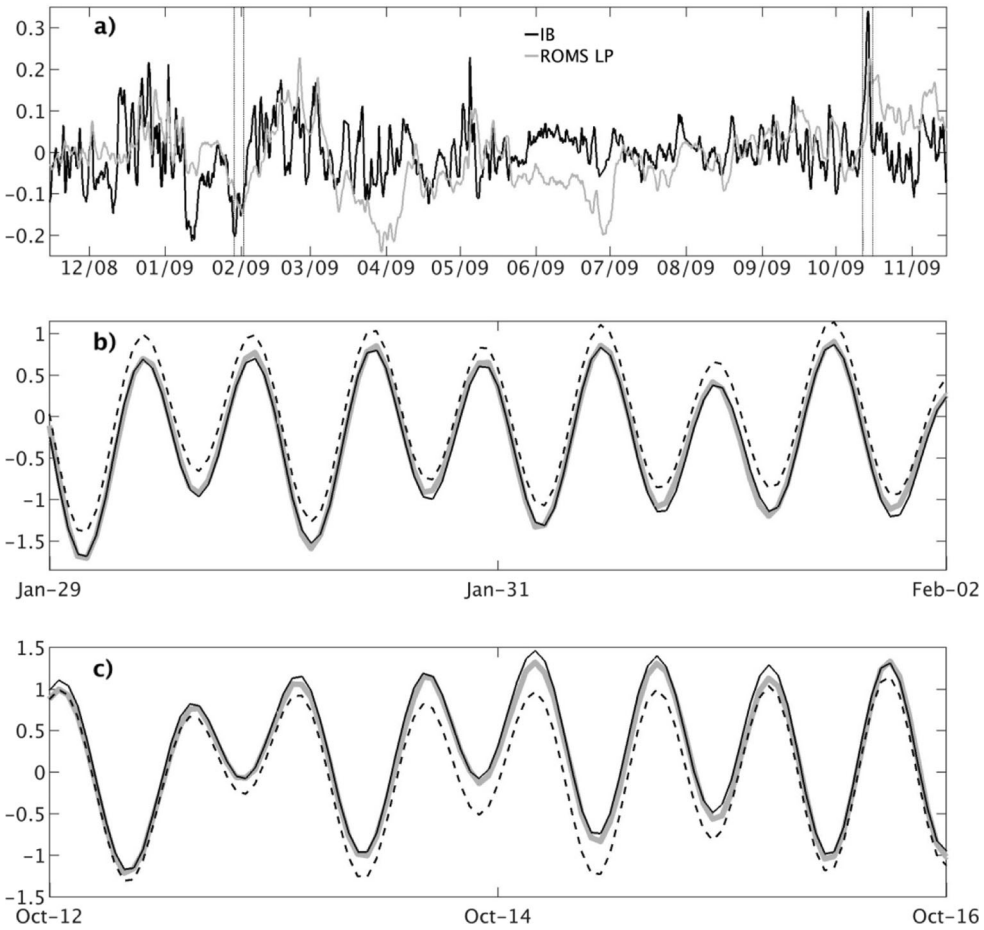

Fig. 2 Time series of coastal sea elevation components at South Beach, OR (m): **a** A 13-month-long time series of ζ_{IB} (*black*) and ζ_{DYN} (*half-tone*); *vertical lines* show time intervals depicted in the panels b and c; *tick marks* along the horizontal axis show the 1st day of each month (month/year); **b**, **c** computed sea elevation time series, including a sum of the 8 tidal constituents (*dashed*) and the total estimate (1) (*solid black*) and total observed (*half-tone*)

bars). Right away, we note that at the 4 locations—Westport, Toke Point, Garibaldi, and Santa Barbara—the total estimates are unsatisfactory low. Analysis reveals that the first three stations are all placed in shallow closed embayments, where the OTIS solution has to be extrapolated and does not provide an accurate estimate for tides. The Santa Barbara Channel in CA (near 34 N) is closed in the OTIS grid and extrapolation from father offshore did not result in a faithful tidal estimate. For these 4 locations, we additionally estimate the tidal harmonics directly from the tide gauge observations and use those instead of OTIS resulting in improved estimates of the total sea level (clear bars on top of the filled ones). Now at each station, F>80% if all terms in (1) are taken into account. At the 12 stations out of the 19, this metric reaches 90% or higher. The tide-only estimate yields F between 60 and 80% in WA, OR, and Northern CA (down to Point Reyes) and is

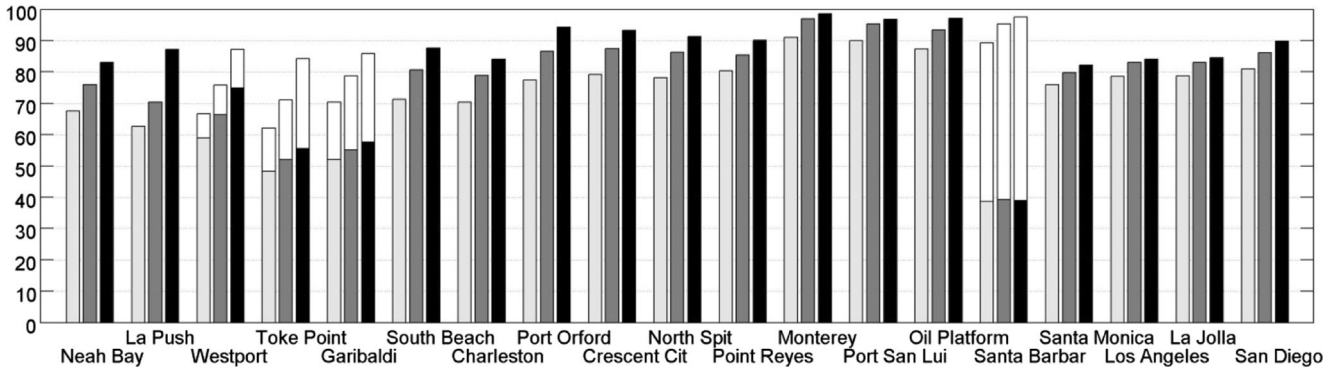

Fig. 3 Frequency of occurrences F of predicted sea level (within 0.15 m of observed) at the tide gauge locations along the West Coast (*left to right*: from north to south): (*light gray*) OTIS tides, (*dark gray*) OTIS tides + ζ_{IB}, (*black*) OTIS tides + ζ_{IB}+ ζ_{DYN}. Estimates using tidal harmonics obtained directly from tide gauge data, instead of OTIS, are shown as white bars (only for the locations where extrapolation of OTIS yielded an unsatisfactory tide estimate)

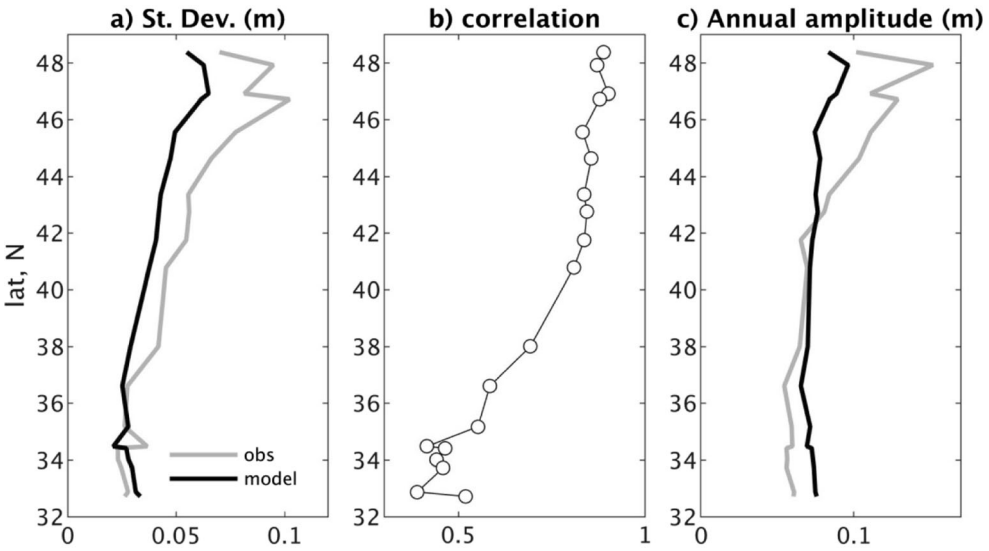

Fig. 4 Model-data statistics for subtidal sea level at the tide gauge locations along the US West Coast: **a** standard deviation in the observed (*half-tone*) and modeled (*black*) *SSHA*, **b** *SSHA* model - tide gauge correlation, **c** the annual constituent amplitude (*half-tone*: observations, *black*: model)

relatively larger (75 to 90%) in Central and Southern California where non-tidal dynamical sea level response and atmospheric pressure variations are generally weaker. The IB effect adds between 5 and 10% to *F*. Depending on location,

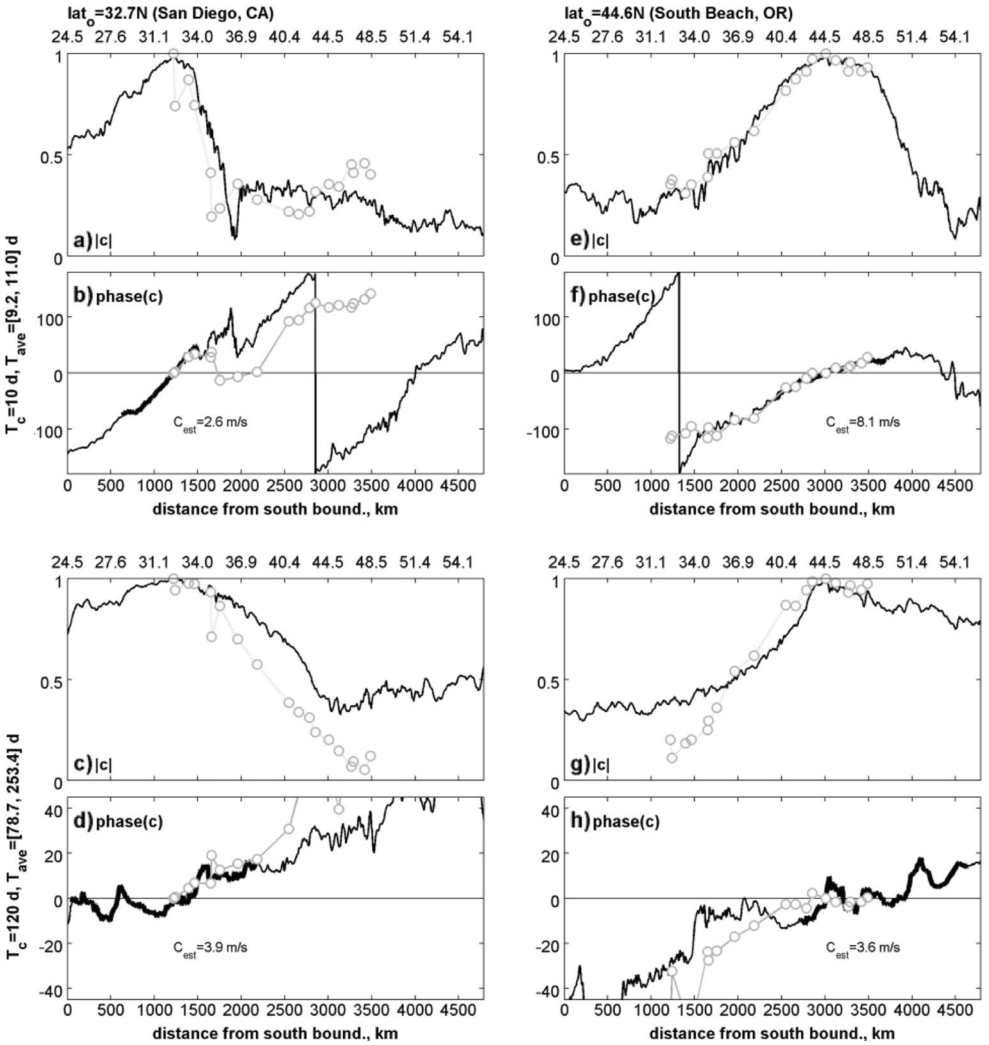

Fig. 5 The amplitude and phase of the alongshore coastal sea level coherence with respect to the reference points at (*left*) 32.7 N (San Diego, CA) and (*right*) 44.6 N (South Beach, OR). The averaging frequency interval is from $\sigma = 1/T_{max}$ to $1/T_{min}$, centered at $1/T_c$: (*top two rows*) $T_c = 10$ days, $[T_{min}, T_{max}] = [9.2, 11.0]$ d, (*bottom two rows*) $T_c = 120$ days, $[T_{min}, T_{max}] = [78.7\ 253.4]$ d. The horizontal axis is the alongshore distance measured from the model southern boundary; the corresponding latitudes are shown on the top of each amplitude plot. Model estimates are shown as *black curves*, and the tide gauge based estimates as *circles*. C_{est} is obtained using model coherence phase estimates in the intervals where $|c| > 0.8$ (shown as *bold lines*)

the ocean dynamics contribution can improve F by as much as additional 5–15%. At each station, the IB term improves F compared to the tide-only estimate, and the ocean dynamic term improves F compared to the estimate based on tides plus IB. The positive impact of the ocean dynamic term is relatively larger in WA and OR. Without a model that predicts correctly response to the winds over the US West Coast shelf, including currents and coastally trapped waves (see discussion below), attaining the recommended level of F=90% would be impossible.

4 Additional comparisons for coastal sea level

Besides being a measurable contributor to the total sea level, $\zeta_{DYN}(t)$ is also an important indicator of processes that define coastal ocean variability at a wide spectrum of temporal scales. In this section, we provide additional verification of the model and observed $\zeta_{DYN}(t)$. To make the data comparable to the 6-year model simulation, the IB correction is subtracted from the data using the 3-h resolution NAM pressure time series, then the 40-h half-amplitude filter is applied to remove tides, and after that, the data are daily averaged.

For further analyses, we would like to evaluate accuracy at intraseasonal temporal scales, between 2 and 60 days. A 60-day half-amplitude low pass filter is applied to the model and observation-based time series. The anomaly SSHA is computed by subtracting these filtered time series from the original detided daily time series. The standard deviation in SSHA (Fig. 4a, half-tone) is close to 0.03 m in Southern and Central CA (32–37 N) and is increasing almost linearly with latitude farther north reaching 0.1 m in WA. The WCOFS estimate (black line) is close to the observed standard deviation in the south, between 32 and 37 N, and is increasing further north, but not as strongly as observed (reaching 0.07 m in WA). The SSHA model-data correlation (Fig. 4b) is between 0.4 and 0.5 in Southern CA. From Central CA to Southern OR (35–41 N), the correlation grows linearly and reaches values of 0.8–0.9 in OR and WA. The increase in correlation may in part be explained by the stronger wind control on the shelf flows in the north and also as a result of SSH variability forced by the winds to the south of a given location and propagating with CTWs to the north. To determine the correlation significance level, we first estimate the lagged autocorrelation, which reduces to essentially zero for 10-day lags at each station. Given more than 2000 points (days) in the time series, the estimated number of degrees of freedom is 200 and the 95% significance level is near 0.1. All along the coast, including Southern CA, the correlations are significant.

The time series were fit using least squares on the combination of the annual and semi-annual harmonics. The

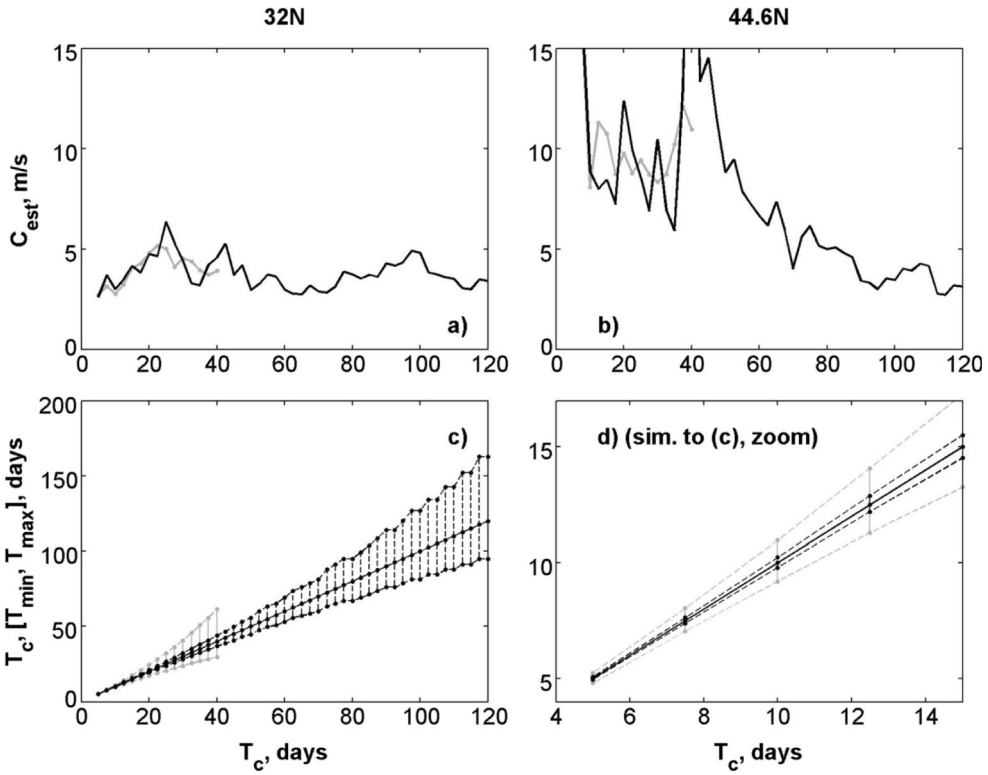

Fig. 6 (*Top*) The alongshore propagation speed C_{est} of the coastal sea level signal estimated using the slope in the coherence phase and shown as a function of the period $T_c = 1/\sigma_c$ corresponding to the center of the frequency averaging interval, for reference locations at: **a** 32 N (Southern California Bight), **b** 44.6 N (mid-Oregon). The averaging intervals are (*half-tone*) $\sigma_c \pm 20\Delta\sigma$ and (*black*) $\sigma_c \pm 5\Delta\sigma$, where $\Delta\sigma = 4.4 \times 10^{-4}$ cycles/day (*bottom*) The corresponding averaging period intervals. **d** A zoom on **c**, in the range of low T_c

model and observation-derived annual amplitudes are comparable between 32 and 42 N and are close to 0.07 m (Fig. 4c). Further north (in OR and WA), the observation-based estimate grows linearly with the latitude to reach 0.15 m at the La Push station (48 N). The model fails to show the same pattern, reaching only 0.09 m at La Push. Additional analysis (not shown), comparing alongshore winds from NAM and a shelf buoy south of Cape Blanco (43.2 N), suggests that the model winds are weaker at that location in summers (e.g., in 2014 the NAM speed is twice as weak as observed, translating in a 4 times as weak wind stress as needed). It is possible that the 12-km resolution atmospheric model has limited ability representing orographic wind intensification south of major capes in the Pacific Northwest (Perlin et al., 2004). If so, this will explain a weaker model SSH response, resulting in lower standard deviations in the 2–60-day band (see Fig. 4a) and the lower annual amplitude (see Fig. 4c). The 4-km resolution NAM real-time forecasts have recently become available. In future studies, we will analyze if the higher resolution atmospheric model yields stronger coastal winds and what effect they have on the coastal sea level.

Vinogradov and Ponte (2010) analyzed annual amplitudes in the tide gauge and satellite altimetry sea level globally and found that the US Pacific Northwest is one of the regions where the estimates at tide gauges are substantially larger than altimetry-based ones at points closest to (about 50 km from) the coast. Similar analyses using WCOFS and altimetry would be interesting to perform, but are left as a topic of future studies. In particular, it will be interesting to evaluate the model against the newly reprocessed alongtrack altimetry that recovers the useful data closer to the coast (Roblou et al. 2011).

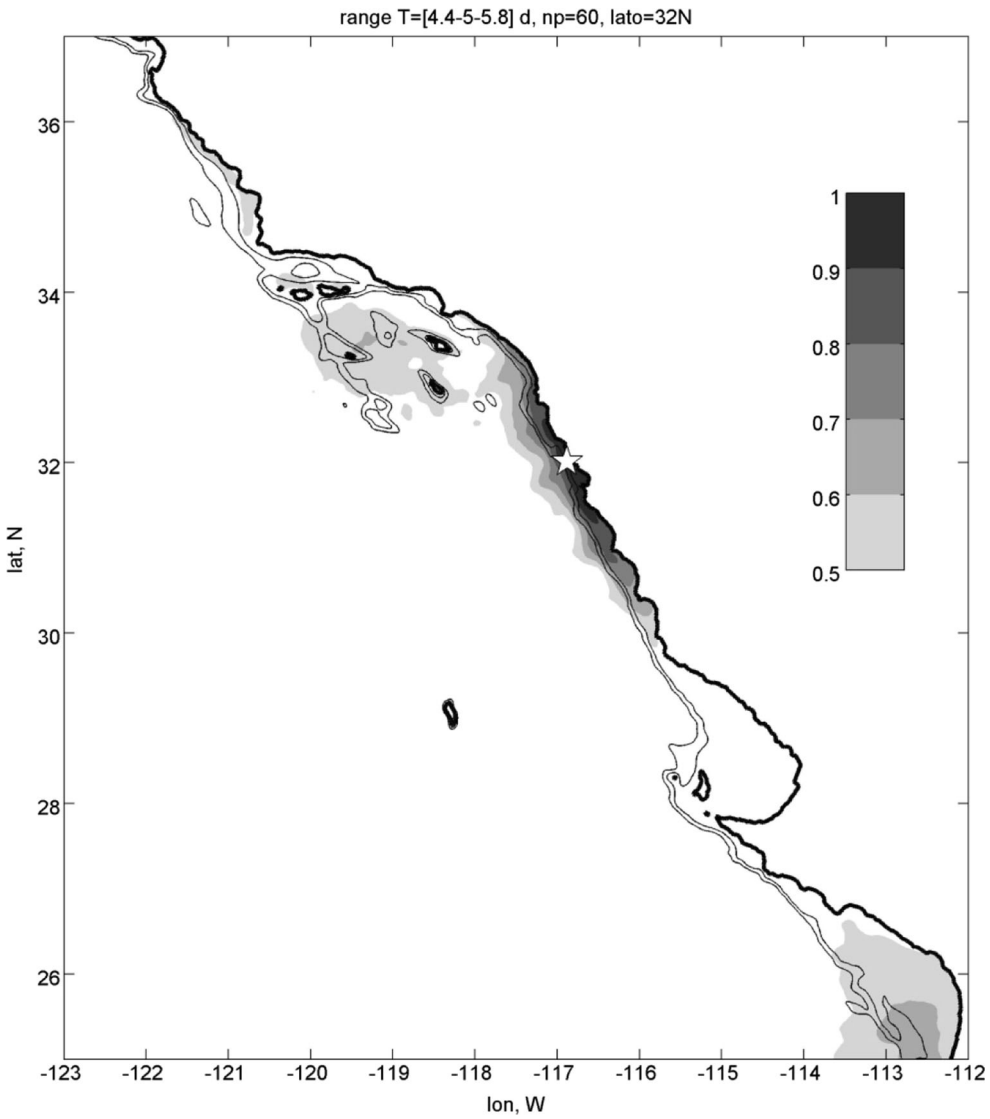

Fig. 7 The SSH coherence amplitude (shades are for $|c| \geq 0.5$) with respect to SSH at the coastal reference point at 32 N (shown as *star*), T_c=5 days, $n = 60$ (4.4 to 5.8 days). Line contours are the coast and 200 and 1000-m isobaths

5 Alongshore coherence

The coherence between two time series $q(t)$ and $z(t)$ is defined as a relation in a specified frequency band (e.g., Kim et al., 2015):

$$c = |c|e^{i\varphi} = \frac{\langle Q(\omega)Z^*(\omega)\rangle}{\langle Q(\omega)Q^*(\omega)\rangle^{1/2}\langle Z(\omega)Z^*(\omega)\rangle^{1/2}}, \quad (2)$$

where $Q(\omega)$ and $Z(\omega)$ are Fourier coefficients of the time series at frequency ω, the asterisk denotes complex conjugate, and angle brackets the average over a specified frequency range.

Along the US West Coast SSH is coherent in part due to the effect of the coastal trapped waves (CTWs). Before we discuss results of alongshore coherence computations using WCOFS SSH, let us provide a short and selective review of a long and rich history of earlier efforts (e.g., Mooers and Smith 1968; Cutchin and Smith 1973; Huyer et al. 1975; Kundu and Allen 1976; Enfield and Allen 1980; Chelton and Davis 1982; Halliwell and Allen 1984, 1987; Allen and Denbo 1984; Battisti and Hickey 1984; Philander and Yoon 1982; Spillane et al. 1987; Denbo and Allen 1987).

The CTWs emerge as free mode solutions of a linear baroclinic problem on the *f*-plane over an alongshore uniform continental slope (Brink 1991). Along the US West Coast, they travel from south to north. Each of the modes has an SSH expression. The first, fastest mode speed is estimated to be typically between 2 and 4 m s^{-1}. The CTWs can be excited by the alongshore winds. Their propagation explains lagged correlation patterns in the observed sea level at the West Coast showing that variability at a given point on temporal scales of several days and longer leads variability at the points father north (see Halliwell and Allen 1984). The slope of the line of the

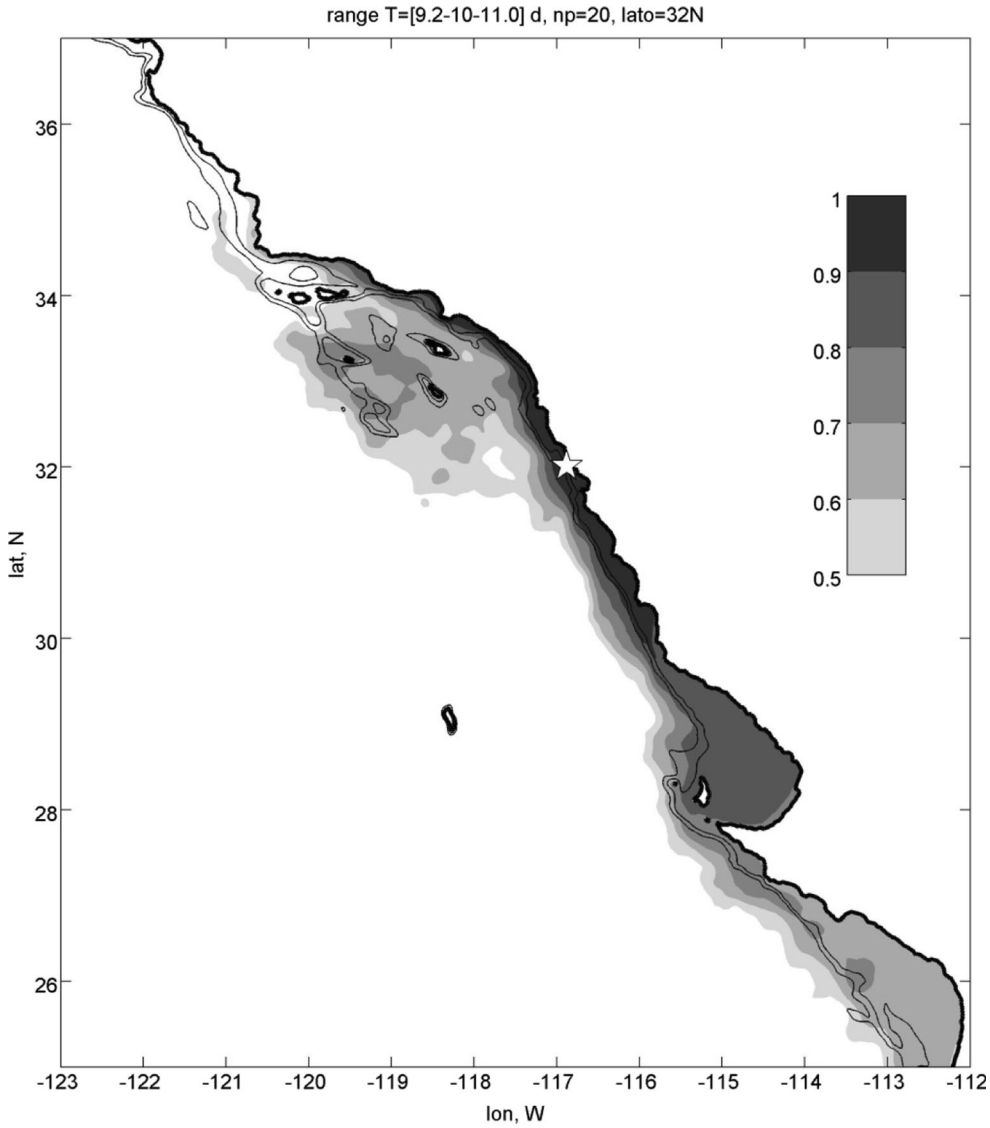

Fig. 8 Sim. to Fig. 7, for a range of longer periods: T_c= 10 days, n = 20 (9.2 to 11 days)

maximum correlation in the alongshore-coordinate-lag/time-lag plane can be taken as an estimate of the propagation speed. It is found to be larger in the Pacific Northwest region (41.8 to 52.2 N) than in California (33 to 41.8 N). Particularly in the north, the propagation speed estimated from the lagged correlation is distinctively larger than the first mode phase speed in the free-wave case. The SSH signal propagation speed can be estimated for a specified frequency interval from the coherence phase of two time series obtained at an alongshore distance y from each other:

$$C_{est} = \frac{\omega}{\alpha} \tag{3}$$

where ω is taken, e.g., in the center of the averaging frequency interval, $\alpha = d\varphi/dy$ is the slope of the coherence phase computed for a series of alongshore points, and the y-coordinate increases in the direction of the wave propagation. The coherence-based estimates of the sea level propagation speed in wind-dominating regions (including Northern CA, OR, and WA) were sensitive to the choice of an analysis time interval and generally larger than the first mode free wave propagation speed. This sensitivity was attributed to differences in wind patterns. For instance, Battisti and Hickey (1984) provided estimates of the coherence in a range of periods between 5 and 20 days for tide gauge records at South Beach (OR) and Neah Bay (WA) using 3 separate 2-month time series. The propagation speed estimates were 5 m s^{-1} in summer 1972, 10 m s^{-1} in summer 1978, and 18 m s^{-1} in winter 1977. The larger speed in winter was explained by the more direct influence of local winds. Enfield (1987) analyzed sea level signal propagation from the Equator to the Eastern Pacific (up to San Francisco in the Northern Eastern Pacific) in a range of longer periods (43–65 days).

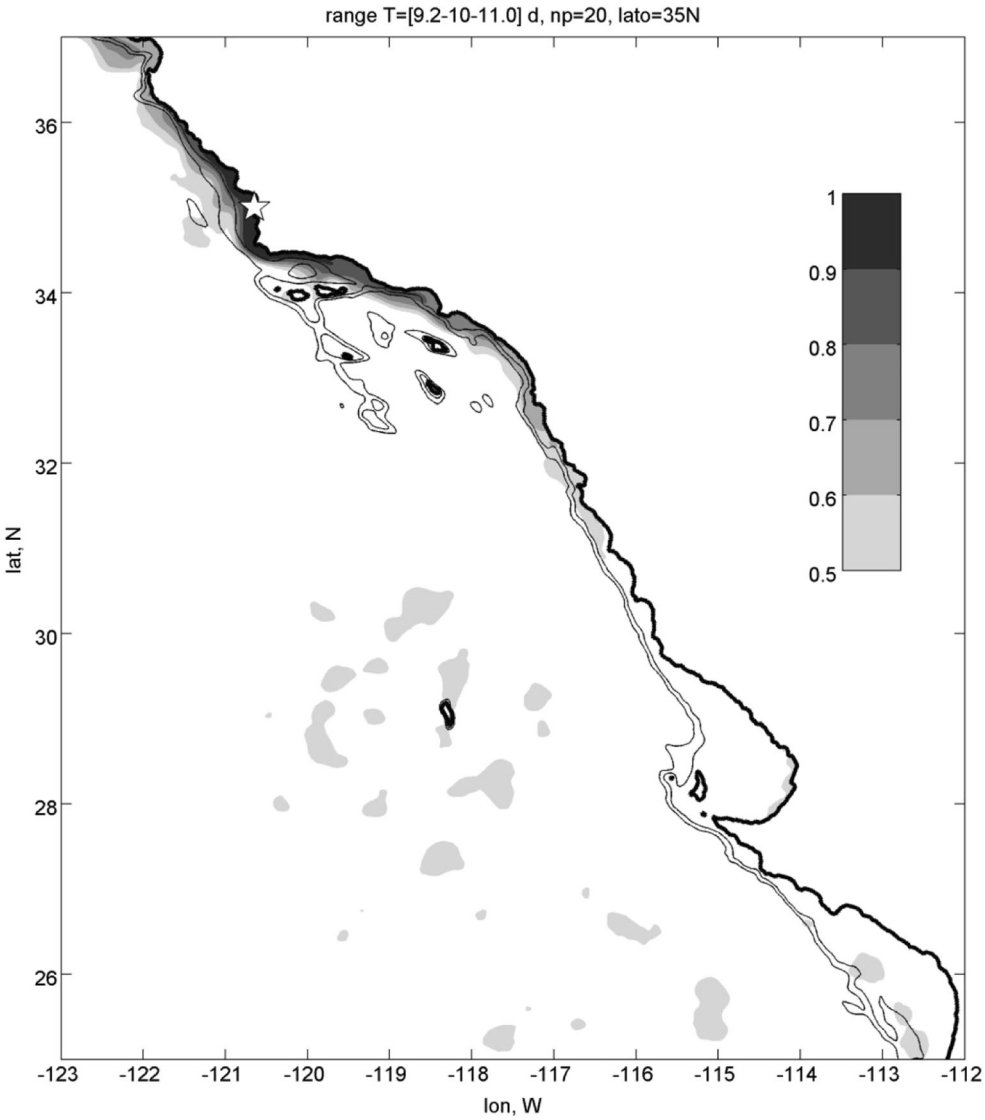

Fig. 9 Sim. to Fig. 8, for the point north of the Santa Barbara Channel. As in Fig. 8, T_c= 10 days, n = 20 (9.2 to 11 days)

The phase speed was found to be close to 3 m s^{-1} in 1982–84 and 5 m s^{-1} in 1980–1982 when the wind influence in the Central Pacific was stronger.

Given the long-wave and low-frequency approximations (i.e., alongshore scales > > the shelf width, time scales > > the inertial period), an appropriate mathematical model of a single CTW mode is a forced, first-order wave equation (Gill and Schumann 1974; Gill and Clarke 1974; Clarke 1977; Brink 1982):

$$\frac{\partial A}{\partial t} + C\frac{\partial A}{\partial y} + \frac{A}{r} = b\tau(y,t) \tag{4}$$

where A is the relevant oceanic variable (e.g., SSH), $\tau(y, t)$ the alongshore wind stress, C the free wave speed, r the frictional time scale, and b is a constant. For a single plane wave solution, satisfying (4) in a case of no friction or wind forcing, the coherence amplitude is 1, the coherence phase φ is changing linearly with y, and $C_{est} = C$.

Halliwell and Allen (1984) demonstrate that (4) describes reasonably well the observed sea level variability along the US West Coast. Allen and Denbo (1984) derive analytical expressions for the space-time lagged correlations and alongshore coherence in A given the assumed statistics of τ, which was consistent with the statistics of the realistic winds in the Pacific Northwest. In particular, they demonstrate that as an effect of the winds, the estimates of the propagation speed based on the lagged correlation or the coherence can exceed C.

The single mode equation was adequate for describing the observed alongshore sea level variability only using a rather high damping rate (e.g., r on the order of 1 day). Including more than one mode in the model (Chapman et al. 1988) yielded good results explaining the observed variability without assuming high damping rates.

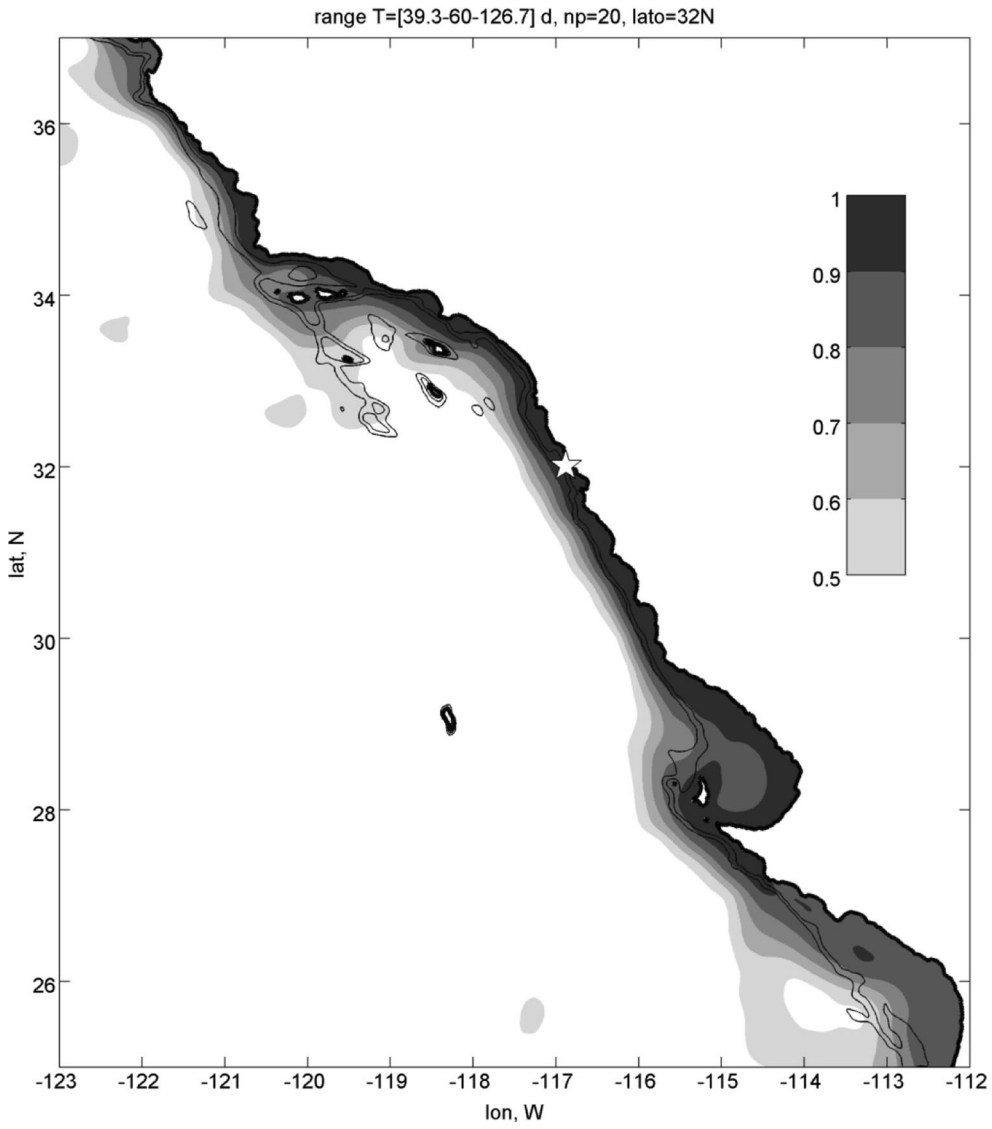

Fig. 10 Sim.to Figs. 7 and 8, for a range of even longer periods: T_c=60 days, n = 20 (39 to 126 days)

Given the 6-year model record, we can compare coherence results for the "weather band", 10–40 days (Halliwell and Allen 1987), and longer period signals (≥60 days). The alongshore coherence of SSH is computed with respect to two reference points, one in the Southern California Bight, where winds are generally weaker, and another in Oregon, where winds are stronger. We will not distinguish between summer and winter regimes and use the full 6-year time series of daily averaged SSH. For these analyses, the model SSH is averaged in the cross-shore direction between the coast and the 500-m isobath, streamlined in regions of complicated bathymetry, e.g., along the outer rim of the Santa Barbara Channel, resulting in the coastal SSH that is only a function of time and the distance from the model south boundary. Spectral decomposition is obtained using the Fast Fourier Transform function in MATLAB, resulting in the coefficients for the frequencies from 0 to 0.5 cpd every $\Delta\sigma = 4.4 \times 10^{-4}$ cpd. The 99% coherence amplitude significance level is determined as 0.5 using D. Kaplan's bootstrap method (http://pmc.ucsc.edu/~dmk/notes/cohere_signif/).

The model and observation-derived coherence amplitude and phase are compared in Fig. 5, for the reference point at San Diego (32.7 N, left) and South Beach, OR (44.6 N, right). The results in the top four panels are for the range of frequencies (1/10) cpd ±20Δσ, corresponding to the 9.2–11.0 days range of periods, and in the lower four panels for a range of (1/120) cpd ±20Δσ, corresponding to the range of very long periods, 79–253 days. Note that if the frequency range is held constant (±20 spectrum points here), the corresponding range of periods is larger for longer period motions. The model- and observation-derived coherence amplitudes match each other in the range of values where the coherence is significant (0.5–1). Phases corresponding to these amplitudes are also comparable. At the location in Southern CA, the shorter-period motions are coherent with those at the south boundary (Fig. 5a). The coherence amplitude falls off much more sharply to the north of the reference point, such that the signal is not coherent with locations north of the Santa Barbara Channel (34.5 N). In the same frequency range, the coastal SSH with respect to the point in OR is coherent with locations to the south, but only to 34.5 N (Fig. 5e). For the longer periods, the coherence amplitude with respect to the location in San Diego is significant with the points farther north, past the Santa Barbara Channel (Fig. 5c).

The average slope of the coherence phase is estimated using model points with $|c| > 0.8$ (thick line segments in Fig. 5b–h). Then the propagation speed estimate (4) is obtained using ω in the center of the frequency averaging interval. For the shorter periods, the estimate in Southern California Bight (2.6 m s^{-1}) is much different from that in OR (8.1 m s^{-1}), which is consistent, e.g., with the findings of Halliwell and Allen (1984). For the range of longer periods, the estimates in the Southern California Bight and OR are much closer, 3.9 and 3.6 m s^{-1} respectively.

Sensitivity of C_{est} to the range of frequencies (periods) is further studied with Fig. 6. Here, C_{est} is computed for a range of frequencies $(1/T_c) \pm n\Delta\sigma$, where T_c is from 5 to 120 days and $n = 5$ (black lines). To check sensitivity to the size of the averaging interval, we additionally show results for T_c from 5 to 40 days and $n = 20$ (half-tone). For reference, the averaging intervals of periods (in units of days) are shown in Fig. 6c and d. For a location at the southern extent of the Southern California Bight (32 N) C_{est} is close to 4 m s^{-1} for the entire range of periods (Fig. 6a). For a location in OR (44.6 N), C_{est} is closer to 10 m s^{-1} for $T_c < 60$ days and is decreasing to values below 5 m s^{-1} for very long periods. The overall behavior of C_{est} as a function of a location and period is consistent with our understanding of the effect of the wind forcing. The estimate of the phase speed is closer to that of freely propagating first mode

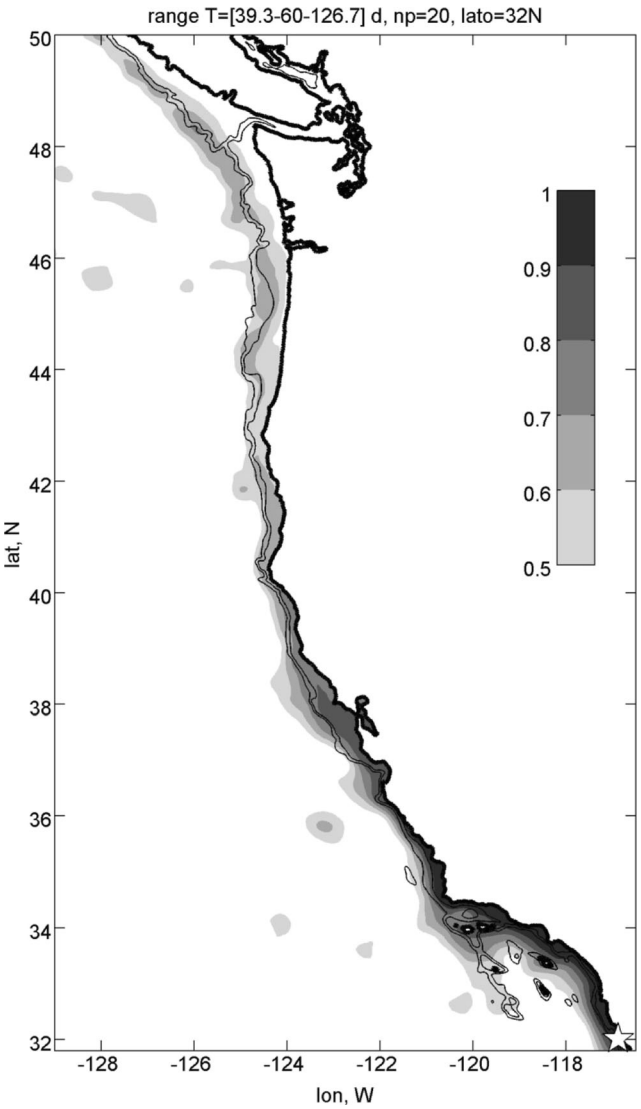

Fig. 11 Sim. to Fig. 10 (i.e., T_c=60 days, $n = 20$ (39 to 126 days)), showing the domain to the north of the reference point (note higher coherence along the shelf break in OR, WA, and BC). *Line contours* are the coast and 200 and 1000-m isobaths

CTWs in the entire range of periods in the south where winds are generally weak and for long periods only (T_c > 60 days, outside the 10–40 day weather band) in the north.

Availability of the model solution offers an opportunity to explore the alongshore and cross-shore coherence structure, by computing two-dimensional coherence amplitude maps. Examples are shown in Fig. 7, 8, 9, 10, and 11, discussed below. Our focus here is on how the coherence pattern survives passing the Santa Barbara Channel. For the coastal reference point is at 32 N, for $T_c = 5$ days (the range of periods 4.4 to 5.8 days, $n = 60$), the signal is coherent only with points between 30 and 33 N. The coherence drops off across the continental slope, which will be a general feature in each case discussed here. The short-period signal is also weakly coherent (0.5–0.6) with interior locations in the area of complicated bathymetry in the Southern California Bight south of Santa Barbara Channel. For twice as long periods, $T_c = 10$ d (9.2–11.0 days, $n = 20$), the coastal sea level at 32 N is strongly coherent with motions to the south all the way to the south boundary (Fig. 8). Areas of the coherent variability are wider over the wider shelf portions in Mexico. To the north, the coherent pattern enters the Santa Barbara Channel. However, it is limited to the northern shore there and does not extend past Point Conception (34.4 N). Strong coherence (albeit a complicated geometrical pattern) is found with interior points south of the Santa Barbara Channel. In this case, over realistic bathymetry, we are unable to track and analyze transformation of CTW modes as they cross the area of the wider shelf. We understand that the first mode CTW scatters, i.e., transfers energy to higher modes (Wilkin and Chapman 1990), and dissipates in the area of and south of the Channel. At the same range of frequencies, we inquire how coherent the shelf SSH is with the coastal location at a short distance north of the channel (Fig. 9). The coherence is significant only along the coast and does not extend to the islands bordering the channel or the continental slope south of the Channel Islands.

Returning at the reference point at 32 N, let us now look at the pattern corresponding to longer periods, $T_c = 60$ days (39.3–127 days, $n = 20$). In the same subdomain as above, focused on Mexico and Southern CA (Fig. 10), SSH is coherent all along the shelf and slope. The coherent pattern is found along the coast and also along the slope south of the Santa Barbara Channel. The coherence is not anymore elevated in the interior zone south of the Channel. At the same range of long periods, the coherence is analyzed farther north (Fig. 11). Computations suggest that the coastal sea level signal at 32 N is coherent with SSH along the *shelf break* along the wider shelf areas in OR, WA, and BC, while being weakly coherent with coastal SSH at the same latitudes.

6 Summary

Although the regional WCOFS model underestimates tidal amplitudes at the coast, it remains a useful predictor of dynamical SSH variability on longer time scales. A practical solution to accurate estimation of the total coastal sea level, evaluated here in terms of the frequency of occurrence metric *F*, consists in combining the tidal estimates from a data assimilative tidal model or available time series observations, the inverse barometer effect using the atmospheric sea level pressure from a numerical prediction model, and the subtidal sea level associated with winds and geostrophic adjustment to alongshore shelf currents, provided by WCOFS. The IB and DYN components add to *F* each providing consistent and sizable improvement to the tide only estimate all along the US West Coast. The subtidal coastal level in WCOFS has been additionally verified against the tide gauge data, in terms of standard deviations (in the 2–60-day band), time correlations, and the annual amplitude. The correlation improves from south to north, both due to the fact that the shelf currents are more directly wind driven in the north and also due to the propagation of CTWs. The annual cycle amplitude in the model is lower than observed in OR and WA. Weaker than observed model coastal winds in summer in particular south of major capes is a possible reason.

The 6-year WCOFS model solution proves to be a useful tool for studies of alongshore connectivity, in part due to its correct performance in terms of the alongshore coherence. The model suggests that at the range of periods around 60 days the coastal sea level in South CA is coherent with the SSH variability over the shelf break in Oregon, Washington, and British Columbia, more than with the coastal SSH at the same latitudes. This will encourage us to look in the future studies at the coherence of SSH and subsurface slope flows. Availability of a multiyear simulation will allow us looking at relatively long-period coastal, shelf, and slope ocean variability and, e.g., their connectivity to intraseasonal variability in the tropics (Maloney and Hartmann 2001).

Acknowledgements We would like to thank Drs. J. S. Allen, K. Brink, and M. Fewings for stimulating discussions and suggestions toward the manuscript improvement. This research was partially supported by the NOAA WCOFS Grant, the NOAA Coastal Ocean Modeling Testbed (COMT) grant, the NASA SWOT Science Definition Team project, and the NSF grant #1030922.

References

Allen JS, Denbo DW (1984) Statistical characteristics of the large-scale response of coastal sea level to atmospheric forcing. J Phys Oceanogr 14:1079–1094

Battisti DS, Hickey BM (1984) Application of remote wind-forced coastal trapped wave theory to the Oregon and Washington coasts. J Phys Oceanogr 14:887–903

Brink K (1982) The effect of bottom friction on low frequency coastal trapped waves. J Phys Oceanogr 12:127–133

Brink KH (1991) Coastal-trapped waves and wind-driven currents over the continental shelf. Ann Rev of Fluid Mech 23:389–412. doi:10.1146/annurev.fl.23.010191.002133

Chapman DC, Lentz SJ, Brink KH (1988) A comparison of empirical and dynamical hindcasts of low-frequency, wind-driven motions over a continental shelf. J Geophys Res 93:12,409–12,422

Chelton DB, Davis RE (1982) Monthly mean sea level variability along the west coast of North America. J Phys Oceanogr 12:757–784

Clarke AJ (1977) Observational and numerical evidence for wind-forced coastal trapped long waves. J Phys Oceanogr 1:231–247

Cutchin DL, Smith RL (1973) Continental shelf waves: low-frequency variations in sea level and currents over the Oregon continental shelf. J Phys Oceanogr 3:73–82

Denbo DW, Allen JS (1987) Large-scale response to atmospheric forcing of shelf currents and coastal sea level off the west coast of North America: May-July 1981 and 1982. J Geophys Res 92:1757–1782

Durski SM, Kurapov AL, Allen JS, Kosro PM, Egbert GD, Shearman RK, Barth JA (2015) Coastal Ocean variability in the US Pacific Northwest region: seasonal patterns, winter circulation, and the influence of the 2009–2010 El Niño. Ocean Dyn 65(12):1643–1663. doi:10.1007/s10236-015-0891-1

Egbert GD, Erofeeva SY (2002) Efficient inverse modeling of Barotropic Ocean tides. J Atmos Ocean Technol 19:183–204

Enfield, D. B., (1987): The interseasonal oscillation in Eastern Pacific sea levels: how is it forced? *J. Phys. Oceanogr.*, 1860–1876.

Enfield DB, Allen JS (1980) On the structure and dynamics of monthly mean sea level anomalies along the Pacific coast of North and South America. J Phys Oceanogr 10:557–578

Erofeeva SY, Egbert GD, Kosro PM (2003) Tidal currents on the Central Oregon shelf: models, data, and assimilation. J Geophys Res 108(C5):3148. doi:10.1029/2002JC001615

Fairall CW, Bradley EF, Rogers DP, Edson JB, Young GS (1996) Bulk parameterization of air-sea fluxes for TOGA COARE. J Geophys Res 101:3747–3767

Gill AE, Clarke AJ (1974) Wind-induced upwelling, coastal currents and sea-level changes. Deep-Sea Res 21:325–345

Gill AE, Schumann EH (1974) The generation of long shelf waves by the wind. J Phys Oceanogr 4:83–90

Halliwell GR Jr, Allen JS (1984) Large-Scale Sea level response to atmospheric forcing along the west coast of North America, summer 1973. J Phys Oceanogr 14:864–886

Halliwell GR Jr, Allen JS (1987) Wavenumber-frequency domain properties of coastal sea level response to alongshelf wind stress along the West Coast of Norh America, 1980-1984. J Geophys Res 92:11, 761–11,788

Huyer A, Hickey BM, Smith JD, Smith RL, Pillsbury RD (1975) Alongshore coherence at low frequencies in currents observed over the continental shelf off Oregon and Washington. J Geophys Res 80: 3495–3504

Kim SY, Kurapov AL, Michael Kosro P (2015) Influence of varying upper ocean stratification on coastal near-inertial currents. J Geophys Res Oceans 120:8504–8527. doi:10.1002/2015JC011153

Kundu PK, Allen JS (1976) Some three-dimensional characteristics of low-frequency current fluctuations near the Oregon coast. J Phys Oceanogr 6:181–199

Kurapov AL, Foley D, Strub PT, Egbert GD, Allen JS (2011) Variational assimilation of satellite observations in a coastal ocean model off Oregon. J Geophys Res 116:C05006. doi:10.1029/2010JC006909

Maloney ED, Hartmann DL (2001) The Madden–Julian Oscillation, barotropic dynamics, and North Pacific tropical cyclone formation. Part I: observations. Mon. Wea. Rev. 58(17):2545–2558

Mass C, Dotson B (2010) Major extratropical cyclones of the Northwest United States: historical review, climatology, and synoptic environment. Mon Wea Rev 138:2499–2526

Mellor GL, Ezer T (1995) Sea level variations induced by heating and cooling: an evaluation of the Boussinesq approximation in ocean models. J Geophys Res 100(C10):20565–20577. doi:10.1029/95JC02442

Mellor GL, Yamada T (1982) Development of a turbulence closure model for geophysical fluid problems. Rev Geophys 20(4):851–875. doi:10.1029/RG020i004p00851

Mooers CNK, Smith RL (1968) Continental shelf waves off Oregon. J Geophys Res 73(2):549–557

Perlin, N., R. M. Samelson, and D. B. Chelton, (2004): Scatterometer and model wind and wind stress in the Oregon–Northern California coastal zone. *Mon. Wea. Rev.*, 2110–2129.

Philander SGH, Yoon J-H (1982) Eastern boundary currents and coastal upwelling. J Phys Oceanogr 12:862–879

Roblou L, Lamouroux J, Bouffard J, Lyard F, Le Henaff M, Lombard A, Marsaleix P, De Mey P, Birol F (2011) Post-processing altimeter data towards coastal applications and integration into coastal models. In: Vignudelli S, Kostianoy AG, Cipollini P, Benveniste J (eds) Coastal altimetry. Springer-Verlag, Berlin. doi: 10.1007/978-3-642-12796-0_9

Shchepetkin AF, McWilliams JC (2003) A method for computing horizontal pressure-gradient force in an oceanic model with a nonaligned vertical coordinate. J Geophys Res 108(C3):3090. doi:10.1029/2001JC001047

Shchepetkin AF, McWilliams JC (2005) The regional oceanic modeling systems (ROMS): a split-explicit, free-surface, topography-following-coordinate oceanic model. Ocean Model 9:347–404. doi:10.1016/j.ocemod.2004.08.002

Spillane MC, Enfield DB, Allen JS (1987) Intraseasonal oscillations in sea level along the west coast of the Americas. J Phys Oceanogr 17: 313–325

Springer SR, Samelson RM, Allen JS, Egbert GD, Kurapov AL, Miller RN, Kindle JC (2009) A nested grid model of the Oregon coastal transition zone: simulations and comparisons with observations during the 2001 upwelling season. J Geophys Res 114:C02010. doi:10.1029/2008JC004863

Vinogradov SV, Ponte RM (2010) Annual cycle in coastal sea level from tide gauges and altimetry. J Geophys Res 115:C04021. doi:10.1029/2009JC005767

Wilkin JL, Chapman DC (1990) Scattering of coastal-trapped waves by irregularities in coastline and topography. J Phys Oceanogr 20:396–421

Wunsch C, Stammer D (1997) Atmospheric loading and the oceanic "inverted barometer" effect. Rev Geophys 35:79–107

Zhang, A., K. W. Hess, E. Wei, and E. Myers, (2006): Implementation of model skill assessment software for water level and current in tidal regions, NOAA Technical Report NOS CS 24, Silver Spring, MD, March 2006 (available online: http://www.nauticalcharts.noaa.gov/csdl/publications/TR_NOS-CS24_FY06_AJ_SkillAssessment.pdf).